Carbohydrate Polymers 205 (2019) 295–301

Contents lists available at ScienceDirect

Carbohydrate Polymers

journal homepage: www.elsevier.com/locate/carbpol

Porous structured cellulose microsphere acts as biosensor for glucose detection with "signal-and-color" output

Wei Li[a,b], Li Zhang[a,*], Qi Li[b], Shenggao Wang[c], Xiaogang Luo[c], Hongbing Deng[d], Shilin Liu[b,*]

[a] Department of Thoracic and Cardiovascular Surgery, Zhongnan Hospital of Wuhan University, Wuhan University, Wuhan, 430071, China
[b] College of Food Science & Technology, Huazhong Agricultural University, Wuhan, Hubei, 430070, China
[c] School of Chemical Engineering and Pharmacy, Wuhan Institute of Technology, Wuhan, Hubei, 430073, China
[d] School of Resource and Environmental Science, Wuhan University, Wuhan, 430079, China

ARTICLE INFO

Keywords:
Biosensor
Cellulose
Plasma grafting
Glucose detection

ABSTRACT

In order to develop a biosensor based on porous structured cellulose microspheres for glucose detection with "signal-and-color" output, in this work, active group carboxyl was introduced to cellulose matrix by using plasma technology, and then glucose oxidase (GOx) was chemically immobilized through EDC-NHS cross-linking reaction. The cellulose microgels containing 21.28 mg/g of enzymes exhibited a fast response to 0.003 M glucose within only 4 min. As for detecting subject with a lower concentration of glucose, the probe still worked. When the concentration of glucose solution was 0.005 M, it took only 2 min that the reaction mixture changed from colorless to yellow. By the introduction of starch, the reaction mixture presented as amaranth color. Besides, the porous-structured substrate and the facile plasma technology were also promising for constructing enzyme-driven catalytic systems with enhanced performance.

1. Introduction

Since understanding glucose level is of great importance in many areas, glucose sensors have attracted substantial research interest in food industry, medical design, diabetes treatment, etc (Belbekhouche, Charaabi, Picton, Cerf, & Carbonnier, 2018; Lee et al., 2016; Peng et al., 2018). Recently, special efforts were directed to design nonenzymatic glucose sensors because they were free from the limitation of enzyme activity (Liu, Hui, & Hui, 2016; Madhu et al., 2015; Zhao et al., 2015). However, the commercialization of the nonenzymatic sensors has been limited for the high cost, poor biocompatibility, time-consuming preparation processes. Thus, additional efforts have being focused on the paper-based functional materials as biosensor and diagnostics due to the low cost and good biocompatibility, but most of paper-based biosensor and diagnostics were macroscopic. (Derikvand, Yin, Barrett, & Brumer, 2016; Liu, Zhu, Li, Li, & Li, 2016; Vashist, Lam, Hrapovic, Male, & Luong, 2014; Wang et al., 2014). The macroscopic analysis systems have various disadvantages when compared with the miniaturized system (also known as "lab-on-a-chip"), for instance, the slower analysis rate, more sample and reagent consumption and lower levels of automation and throughput (Srinivasan, Pamula, & Fair, 2004). Our team had put intensive researches on the modification and application of micronized cellulose, and the cellulose microgel prepared from alkaline/urea aqueous solution was found having porous structure and higher surface area-to-volume ratio than normal papers (Li et al., 2016, 2017).

Glucose oxidase (GOx) and peroxidase (HRP) are the commonest enzymes for glucose detection of blood, urine, sweat, saliva, tears, and exhaled air (Cha, Jensen, Balijepalli, Cohan, & Meyerhoff, 2014; Hu, Jiang, Zhang, Fan, & Wu, 2013; Liu, Sun, Shang, Lai, & Zhang, 2016; Peng et al., 2013; Shen & Xia, 2014; Yan et al., 2013). The GOx can reduce oxygen to hydrogen peroxide and simultaneously transform glucose to D-glucono-1, 5-lactone, and HRP catalyzes the oxidation of iodide by hydrogen peroxide and generates yellow color (iodine) (Riccardi et al., 2016; Su et al., 2012; Wei & Wang, 2008; Wooten, Karra, Zhang, & Gorski, 2013). Riccardi et al. presented an interest work, and it indicated that covalent interlocking of GOx and HRP with polyacrylic acid in the voids of paper had a good catalytic effect for glucose detection (Riccardi et al., 2016). However, without chemically modifying cellulose with carboxyl groups, the stability and long-lasting effect was doubtable in this case. While low temperature plasma technique is an attractive technology to chemically modify cellulose since it is simple, quick and widely used in surface functionalization of polymers (Sun et al., 2010). One serious drawback of the plasma technique is the time dependency of the surface properties of plasma-treated polymers. The method to avoid the drawback is to graft monomers on

* Corresponding authors.
E-mail addresses: zl0104@whu.edu.cn (L. Zhang), slliu2013@mail.hzau.edu.cn (S. Liu).

https://doi.org/10.1016/j.carbpol.2018.10.084
Received 13 August 2018; Received in revised form 24 October 2018; Accepted 24 October 2018
Available online 26 October 2018
0144-8617/

the surface of plasma-treated polymer for the "lock-in" chemistry, which is the so-called plasma-induced grafted polymerization, so that the grafted polymer layers which are chemically bonded to the surface are more stable (Wavhal & Fisher, 2002).

In this work, cellulose microgels with high porosity of 94% were used as the matrix. The monomer of acrylic acid (AA) was polymerized into the cellulose microgels matrix by plasma-induced grafted polymerization, and then the amino groups of GOx and HRP were covalently bonded with the carboxyl groups of the modified cellulose microgels through 1-ethyl-3-(3-dimethylaminopropyl)-carbodiimide (EDC)/ N-hydroxysuccinimide (NHS) cross-linking reaction (Blaik, Lan, Huang, & Dunn, 2016). As mentioned above, the obtained probe was expected to generate yellow color (iodine) in the presence of glucose. Iodine could form a blue complex with amylose and a red complex with amylopectin, therefore, with the introduction of starch, the glucose probe herein was expected to have a dual-color colorimetric reaction.

2. Experimental

2.1. Materials

Native cellulose (cotton linter pulp, α-cellulose ≥95%) was obtained from Hubei Chemical Fiber Co. Ltd. (Xiangfan, China). Its molecular weight (M_w) was determined to be 1.07×10^5 g/moL by using viscosity measurement in cadoxen solvent at 25 °C and the calculation was relied on the Mark-Houwink equation ($[\eta] = KM^{\alpha}$, K = 0.0385, α = 0.76) (Brown & Wikström, 1965). Acrylic acid (AA), paraffin oil, glucose oxidase (GOx), peroxidase (HRP), 1-ethyl-3-(3-dimethylaminopropyl)-carbodiimide (EDC) and N-hydroxysuccinimide (NHS) were purchased from Aladdin Reagent Database Co., Ltd (Shanghai, China). The total protein quantification kit (Coomassie Brilliant Blue) was purchased from Nanjing Jiancheng Bioengineering Institute (Nanjing, China). Other chemicals at analytical grade were purchased from the Sinopharm Chemical Reagent Co., Ltd (Shanghai, China).

2.2. Preparation of regenerated cellulose microgels

The freezing-thawing method was used for the preparation of cellulose solution. Briefly, native cellulose (4.3 wt%) was dispersed into aqueous LiOH/urea solution (4.6 wt%/15.0 wt%). Then put it in a refrigerator at −20 °C for 12 h, afterwards, took it out and thawed at room temperature to obtain the cellulose fluid. The resultant cellulose solution was subjected to centrifugation (7000 rpm at 4 °C for 8 min) to eliminate some bubbles in the viscous solution. Then 40 mL of the cellulose solution was dropped into a well-mixed suspension containing 200 mL of paraffin oils, 3 g of Span 80 and 1 g of Tween 80. After well-proportioned mechanical stirring for 3 h, dilute hydrochloric acid (10%) was added immediately until the pH of resultant suspension reached to 7, then the regenerated cellulose microgels (RCMs) were obtained and washed thoroughly with deionized water and hot ethanol to get rid of paraffin oil, inorganic salt or surfactants.

2.3. Plasma-induced graft polymerization

The RCMs were immersed in 30% (v/v) AA monomer for 30 min., and the AA monomer was purified by the reduced pressure distillation to remove inhibitors before using. Then the RCMs were filtered and vacuum-dried to remove most moisture, and subsequently placed in a glow discharge plasma reactor (SY-DT03, Suzhou OPS Plasma Technology Co., Ltd.). The pressure of reaction chamber was reduced to 10 Pa, which was followed by the introduction of argon gas in the chamber and the pressure increased, then the pressure was decreased to 10 Pa again, and the process was repeated for three times. Next, the microgels were operated at a frequency of 13.56 MHz and an argon flow rate of 50 sccm for 60 s. The modified cellulose microgels were thoroughly washed with deionized water, and then freeze-dried. The obtained cellulose microgels, respectively, were coded as PAC50, PAC100, PAC200 according to the operating power of 50 W, 100 W, and 200 W.

2.4. EDC-NHS chemistry and enzyme attachment

The PAC microgels that contained carboxylate groups could react with amine-rich enzyme through EDC-NHS chemistry (Blaik et al., 2016). Briefly, 0.05 g of RCMs or PAC microgels were mixed with 2 mL of 5.73 mg/mL EDC and 5 mL of 3.26 mg/mL NHS, each in 20 mM MES buff ;er (pH 5.5). After activation at room temperature for 30 min, 1 mL of GOx (0.8 mg/mL) and 1 mL of HRP (2.5 mg/mL) were added, and the reaction was lasted for 2 h. Then the PAC microgels immobilized with enzymes (PACE) and RCMs loaded with enzymes (RCE) were filtered and washed thoroughly with deionized water, finally the PACE and RCE microgels were lyophilized. The PACE microgels were coded as PAC50E, PAC100E, and PAC200E, respectively, according to the initial use of PAC50, PAC100, and PAC200 microgels.

2.5. Characterizations

The surface morphology and porous structure of freeze-dried microgels were characterized by using scanning electron microscope (SEM, TM3030, Hitachi Ltd., Japan). Nitrogen adsorption-desorption isothermals of RCMs and PAC microgels were performed at 77 K by using Brunauer-Emmett-Teller method (BET, ASAP2020, Micromeritics Inc). For the next characterizations, samples were grounded into powders and dried in vacuum oven for 12 h. X-ray photoelectron spectroscopy (XPS) was carried out to identify the existence of atoms on the sample surface by using an axis ultra DLD apparatus (Kratos, UK). Fourier transform infrared (FT-IR) spectra (170-SX, Thermo Nicolet Ltd., USA) were recorded in the wavenumber ranged from 4000 to 400 cm^{-1}, and the number of FTIR scans was 64 times.

2.6. The content of encapsulated enzyme assay

The encapsulating content of enzyme in PACE microgels was determined by the reduced amount of enzyme in the supernatant. The total protein quantification kit (Coomassie Brilliant Blue) was employed to examine the protein concentration in the supernatant before and after the process of enzyme attachment. The RCMs and 30% AA solution, treated with EDC-NHS chemistry and enzyme attachment, were regarded as control samples. The experiment (content of encapsulated enzyme assay) of each sample was repeated for three times.

2.7. Enzymatic colorimetric activity assay

Colorimetric enzymatic activity was measured by the addition of potassium iodide (1 M, 1 mL) to the PACE microgels (0.01 g). Upon the addition of glucose (0.5–50 mM), hydrogen peroxide and gluconic acid were produced with GOx. Then the HRP and hydrogen peroxide oxidize potassium iodide to elemental iodine (colorless to yellow color), and the absorbance was determined by using UV–vis spectrometer (UV-1800, Shimadzu, Japan) for quantitative analysis.

3. Results and discussion

3.1. Microstructure of cellulose microgels before and after being modified

As shown in Fig. 1a, RCM had spherical shape with the diameter about 400 μm. The SEM images showed that RCM had polyporous structures. The PAC microgels also had spherical shape with a porous structure, and the surface morphology was rougher due to the grafted polyacrylic acid, and the grafted polymer resulted in smaller pore size and denser networks in the modified cellulose microgel matrix. Fig. S1 showed the image of more cellulose microgels, it could be seen that all

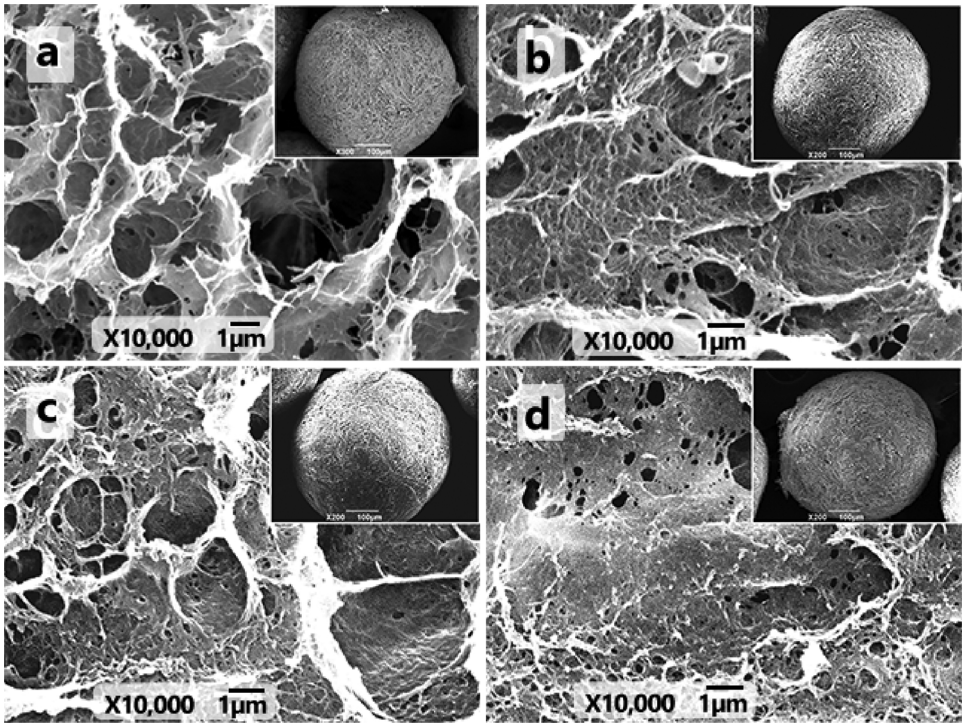

Fig. 1. SEM images and the surface morphology of regenerated cellulose microgels and plasma-modified cellulose microgels: (a) RCM, (b) PAC50, (c) PAC100 and (d) PAC200. The scale bar of the insert figure is 100 μm.

of the microgels had the round shape with porous structure. Nitrogen adsorption-desorption isotherm of RCMs and PAC microgels indicated that the microgels has a clear type H3 hysteresis loop, implying that the microgels before and after modification were both macroporous materials (Fig. S2). The change in pore size distribution and BET surface area indicated that the pore structure of PAC microgels was different from that of RCMs (Fig. S2).

The FT-IR spectra of RCMs and PAC microgels were shown in Fig. 2. According to the spectrum of RCMs, the peak at 3284 cm^{-1} was ascribed to the broad −OH vibration (Li et al., 2014). The peaks for the C−H stretching in glucose units and the antisymmetric bridge C−O−C stretching vibration were at 1384 cm^{-1} and 1165 cm^{-1}, respectively. The peak at 1070 cm^{-1} represented for the C−O stretching of 3,6-anhydrogalactose (Moura, Mattoso, & Zucolotto, 2012; Pereira, Amado, Critchley, van de Velde, & Ribeiro, 2009). The characteristic peak of PAC microgels at 1733 cm^{-1} was due to the C═O stretching (Shan et al., 2009), and the small peak at 551 cm^{-1} was related to the rocking COO− vibration (Caroline, Kandasamy, Mohan, & Vasudevan, 2009), indicating the existing of PAA in the cellulose matrix. Besides, the peaks at 1070 cm^{-1} and 1165 cm^{-1} were sharper, indicating the existence of C−O and C−O−C groups in PAC microgels. In the spectra of PAC microgels from different operating power (Fig. S3), all peaks were at the same wavenumbers with different intensity. All the results supported that the PAA polymer was introduced in the cellulose matrix successfully.

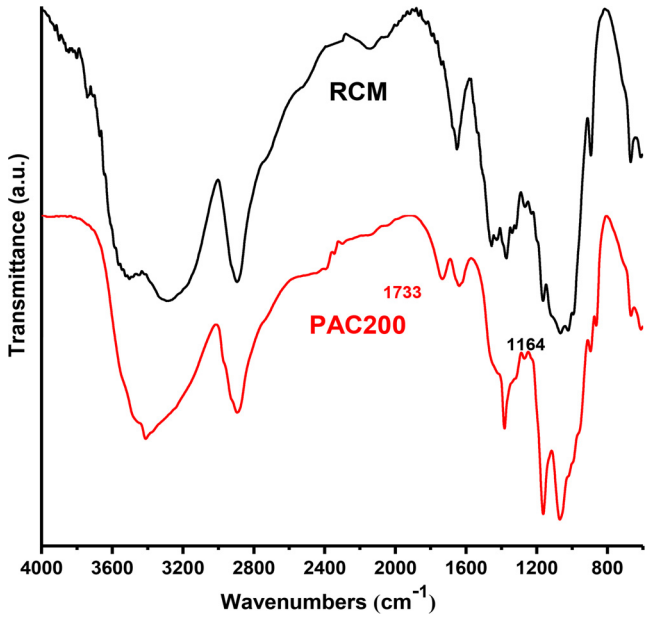

Fig. 2. The FTIR spectra of regenerated cellulose microgels and plasma-modified cellulose microgels.

To investigate the change of surface elemental composition in RCMs, PAC and PACE microgels, XPS analyses were performed and the results were shown in Fig. 3. The strong C_{1s} peak was obvious in all samples, while the extra N_{1s} peak in PACE microgels confirmed that GOx and HRP were successfully grafted onto cellulose matrix. As for RCMs, the high-resolution signal of C_{1s} contained three peaks described as below: the peak at 283 eV was assigned to the hydrogenated sp^2 C−C bond (Wu et al., 2005), the energy position of C_{1s} was at 284 eV for sp^2 C−C bond (Bagus, Ilton, & Nelin, 2013), and the peak at 286 eV was characteristic of carbon adjacent to oxygen (C−O) (Hong, Fischer, Emrick, & Rotello, 2005). In the C1s high-resolution spectrum of PAC microgels, the extra peak at 288 eV (C═O) was coincided with the result of FTIR spectrum and supported the evidence of successfully grafting AA onto cellulose (Cai & Song, 2007). The C_{1s} high-resolution spectrum of PACE microgels had five peaks. Apart from the four peaks mentioned above, the peak at 285 eV was related to the sp^2 C atoms bonded with nitrogen (C−N) (Luo et al., 2011). Besides, the high-resolution spectrum of N_{1s} had one characteristic peak centered at 399 eV. The result of XPS analyses confirmed the enzyme had been successfully introduced on cellulose matrix.

Fig. 4 showed the SEM images of PACE microgels, the microstructure of the microgels was different from that of RCMs and PAC

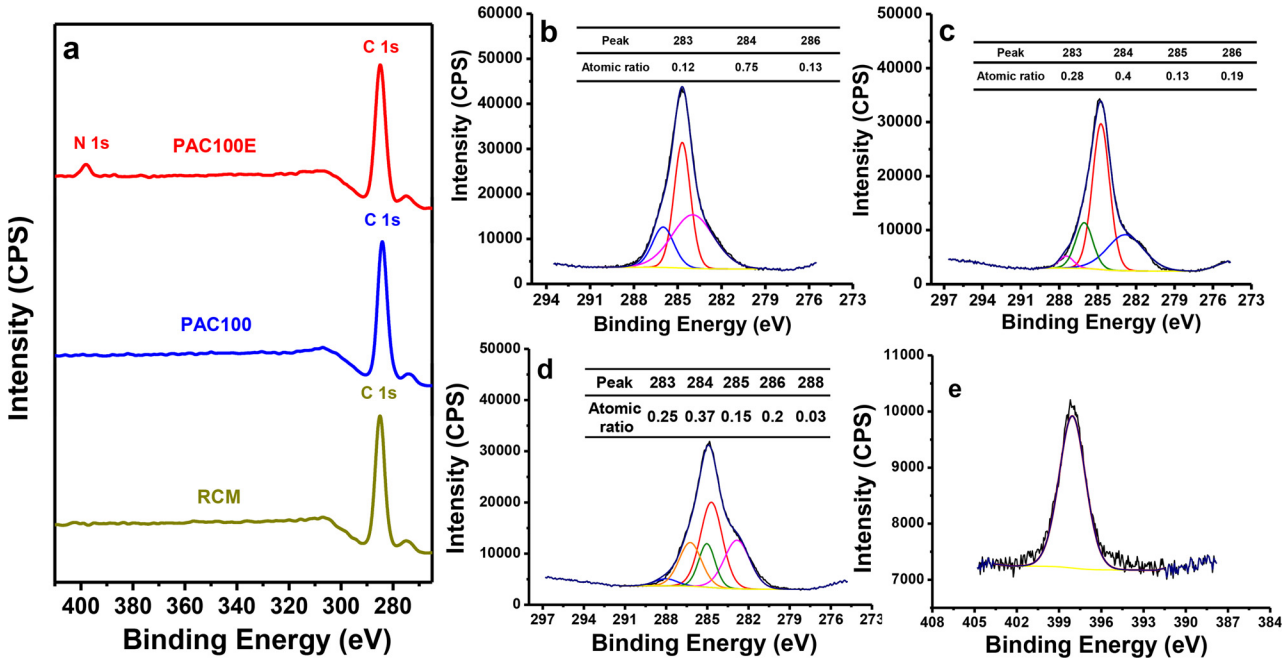

Fig. 3. (A) XPS wide scan with the curve fit of RCM, PAC100 and PAC100E.C_{1s} high-resolution spectra of (b) RCM, (c) PAC100, (d) PAC100E, and N_{1s} high-resolution spectrum of (e) PAC100E.

microgels as it was shown in Fig.1. With the increasing of operating power, the roughness of PACE microgels was increased, and the formed denser structure was due to a thick layer of crosslinked enzymes.

The contents of encapsulated enzymes in PACE microgels were shown in Fig. 5a. Obviously, PAC200E microgels had the largest content of encapsulated enzymes with 21.28 mg/g, closely followed by the PAC100E microgels with 20.42 mg/g and PAC50E microgels with 16.49 mg/g. It indicated that the content of encapsulated enzyme in PACE microgels was increased with the increasing of operating power. It was worth noting that the content of enzymes that mainly encapsulated by physical absorbance in RCE microgels was only about 2.43 mg/g. The chemically crosslinked enzymes in PACE microgels could be indirectly reflected by the comparison between the total content of encapsulated enzymes in PACE microgels and the amount of absorbed enzyme in RCE microgels. The AAE solution treated with the same process of EDC chemistry and enzyme attachment showed no change of enzyme amount in the mixture before and after enzyme attachment process, and it indicated that free AA had little influence on the content of encapsulated enzyme. In the presence of glucose, the encapsulated enzymes could catalyze the oxidation of potassium iodide and generate yellow color (iodide, I_2), which was characterized with a UV–vis spectrometer, so the microgels encapsulated with GOx and HRP could be used as colorimetric probes for glucose detection. As shown in Fig. 5b, the spectrum of RCM had no characteristic peak, while that of other samples exhibited characteristic peak located at 353 nm. The absorbance was directly coincided with the intensity of color, which indicated the amount of the formed I_2 in the reaction mixture. Apparently, the absorbance of the supernatant of PAC200E reaction mixture was the largest within 2 min, followed by PAC100E, PAC50E, and RCE. Based on the results, it indicated that higher operating power led to the higher grafting efficiency of PAA in cellulose matrix, which was resulted in the increased content of encapsulated enzyme. Besides, the higher content of enzyme encapsulated in the porous structured microgels, the higher catalytic efficiency was obtained.

3.2. Performance in the glucose detection

To further explore the catalytic performance, kinetics of enzyme reaction was investigated by detection of colorimetric change over time, and the data was shown in Fig. 6A. The reaction mixture was colorless at first and become light yellow after 1 min, and the yellow color became darker when the reaction time increased. Fig. 6B shows the quantitative analysis of kinetic color change of the catalytic reaction mixture. The absorption of the characteristic peak was lower than 0.3 in 1 min, and it increased to about 0.6 in 2 min, then it got rise to 1.2 within 3 min. When the supernatant of the reaction mixture was diluted to 10-fold, the adsorption was gradually increased, which was coincided with the result of Fig. 6A and C. When compared with the work from Riccarde et al. (Riccardi et al., 2016), the responding time was decreased from 15 min to 2 min, the difference would be resulted from the porous structure of cellulose matrix used. As for Fig. 6C, starch (containing amylopectin and amylose) was added to further study the color change over time. The obvious amaranth sediment was the starch-iodine complex, manifesting the presence of iodine. It indicated that the

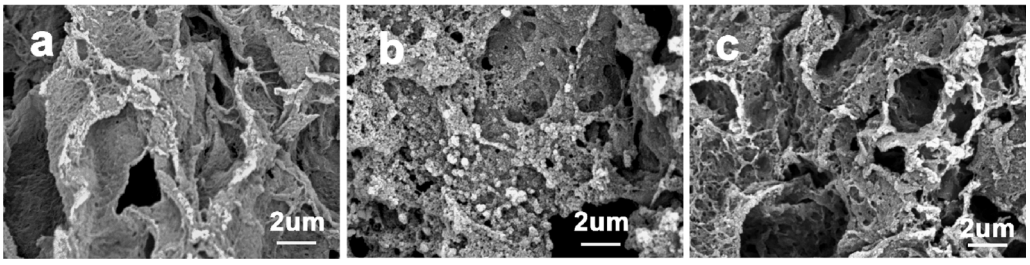

Fig. 4. SEM images and the surface morphology of plasma-modified cellulose microgels loaded with HRP and GOx: (a) PAC50E, (b) PAC100E and (c) PAC200E.

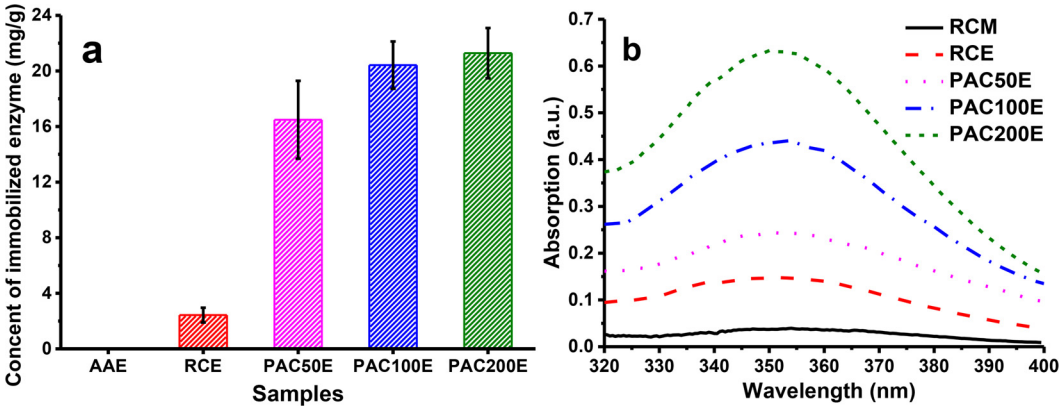

Fig. 5. Panel a represents the content of encapsulated enzyme in PACE microgels. The RCMs and 30% AA solution, treated with EDC-NHS chemistry and enzyme attachment, were regarded as control samples. Panel b is the effect of different colorimetric probes on the UV–vis spectra of the supernatant of reaction mixture (0.05 M glucose solution, 1 M potassium iodide) at 2 min.

porous structure of regenerated microgels contributed to the larger efficient reaction area, thus leading to the faster color change.

The sensitivity and detection range of colorimetric assay were further performed by using different concentrations of glucose solution. As shown in Fig. 7, the higher concentration of glucose solution resulted in stronger absorbance. There was no obvious absorbance for the glucose solution with the concentration of 0.001 M and 0.002 M at 4 min, while for the glucose solution with concentration of 0.003 M, the absorbance value at 353 nm was about 0.15. Afterwards, the absorbance got rise when the concentration of glucose solution was increased, and the intensity of the characteristic absorption peak was increased. In 4 min, the detection limit of glucose concentration was 0.003 M, which is

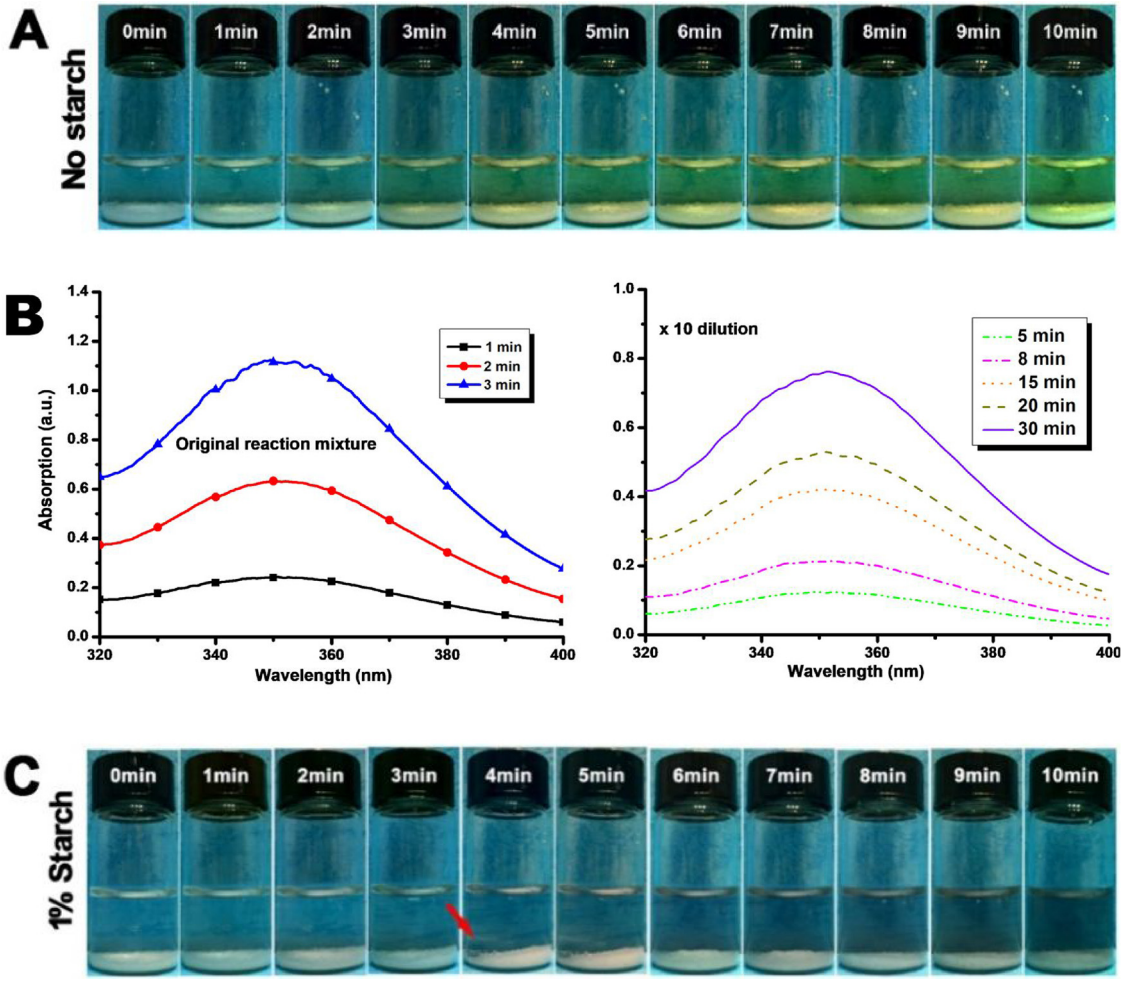

Fig. 6. (A) Colorimetric change of reaction mixture (PAC200E, 0.05 M glucose solution, 1 M potassium iodide) over time; (B) Enzymatic kinetic traces drawn from the UV–vis absorption spectra of the supernatant of reaction mixtures in panel (A), and the mixtures were 10-fold diluted after 4 min in order to make the result precise; (C) Colorimetric change of reaction mixture (PAC200E, 0.05 M glucose solution, 1 M potassium iodide) over time, and the starch is insoluble at room temperature, so most of amaranth complex deposited in the bottom.

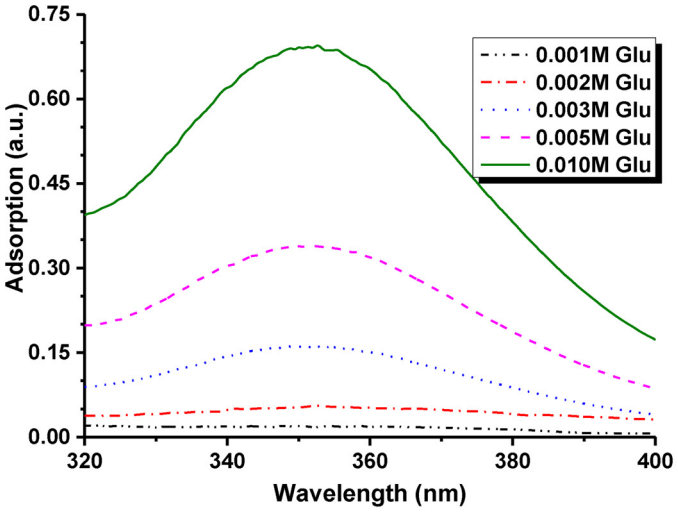

Fig. 7. The change of UV–vis spectra induced by the addition of different concentration of glucose in the presence of PAC200E and 1 M potassium iodide within 4 min, and the pictures on the right showed the colorimetric change of reaction mixture (PAC200E, 0.001 M glucose solution, 1 M potassium iodide) at 30 min and 60 min.

lower than that in a previous work (Riccardi et al., 2016). The improvements in shorter response time and lower detection limit were mainly due to the advantage of micronized cellulose with polyporous structure, which provided more effective areas for immobilizing enzymes and catalytic reaction to detect glucose. As demonstrated in Fig. 6, the reaction degree was increasing over time. The color change of reaction mixture containing 0.001 M glucose solution at 30 min and 60 min was shown in the inset picture of Fig. 7. It demonstrated that the detectability of samples with low glucose concentration (lower than 0.003 M) was also feasible.

4. Conclusion

In this work, the matrix properties of cellulose microgels were modified by plasma-induced grafting polymerization and EDC-NHS cross-linking reaction to encapsulate GOx and HRP for quick and advanced colorimetric glucose detection. The morphology of resultant samples was spherical shape with 3D porous structure, which was significantly affected by the operating power of plasma technology. The driving forces of encapsulated enzyme were divided into two kinds: physical adsorption and chemical crosslinking. The content of physically encapsulated enzyme was only 2.43 mg/g, while for the chemically crosslinking enzyme, the content of the encapsulated enzyme in cellulose matrix could be increased to 18.85 mg/g. When it was applied for glucose detection, the colorimetric probe with a larger content of encapsulated enzyme led to the darker color of the reaction mixture within 4 min, the detection limit of glucose concentration in 4 min was 0.003 M, and as for detecting a lower concentration of glucose, longer time was needed. Besides, the introduction of starch provided an alternative color choice for some special samples like urine, which could greatly reduce the detection error in this case. The resulting platform in this work was a good choice for constructing other enzyme-polymer composites with enhanced performance, which could be applied to various catalytic systems depending on the selection of enzymes.

Acknowledgements

This work was supported by the Wuhan Youth Science and Technology Plan (2016070204010096) and the fund of the Beijing Engineering and Technology Research Center of Food Additives, Beijing Technology & Business University (BTBU).

Appendix A. Supplementary data

Supplementary material related to this article can be found, in the online version, at doi:https://doi.org/10.1016/j.carbpol.2018.10.084.

References

Bagus, P. S., Ilton, E. S., & Nelin, C. J. (2013). The interpretation of XPS spectra: Insights into materials properties. *Surface Science Reports, 68*(2), 273–304.

Belbekhouche, S., Charaabi, S., Picton, L., Cerf, D., & Carbonnier, B. (2018). Glucose-sensitive polyelectrolyte microcapsules based on (alginate/chitosan) pair. *Carbohydrate Polymers, 184*, 144–153.

Blaik, R. A., Lan, E., Huang, Y., & Dunn, B. (2016). Gold-coated M13 bacteriophage as a template for glucose oxidase biofuel cells with direct Electron transfer. *ACS Nano, 10*(1), 324–332.

Brown, W., & Wikström, R. (1965). A viscosity-molecular weight relationship for cellulose in cadoxen and a hydrodynamic interpretation. *European Polymer Journal, 1*(1), 1–10.

Cai, D., & Song, M. (2007). Preparation of fully exfoliated graphite oxide nanoplatelets in organic solvents. *Journal of Materials Chemistry, 17*(35), 3678–3680.

Caroline, M. L., Kandasamy, A., Mohan, R., & Vasudevan, S. (2009). Growth and characterization of dichlorobis l-proline Zn(II): A semiorganic nonlinear optical single crystal. *Journal of Crystal Growth, 311*(4), 1161–1165.

Cha, K. H., Jensen, G. C., Balijepalli, A. S., Cohan, B. E., & Meyerhoff, M. E. (2014). Evaluation of commercial glucometer test strips for potential measurement of glucose in tears. *Analytical Chemistry, 86*(3), 1902–1908.

Derikvand, F., Yin, D. T., Barrett, R., & Brumer, H. (2016). Cellulose-based biosensors for esterase detection. *Analytical Chemistry, 88*(6), 2989–2993.

Hong, R., Fischer, N. O., Emrick, T., & Rotello, V. M. (2005). Surface PEGylation and ligand exchange chemistry of FePt nanoparticles for biological applications. *Chemistry of Materials, 17*(18), 4617–4621.

Hu, Y., Jiang, X., Zhang, L., Fan, J., & Wu, W. (2013). Construction of near-infrared photonic crystal glucose-sensing materials for ratiometric sensing of glucose in tears. *Biosensors & Bioelectronics, 48*, 94–99.

Lee, H., Choi, T. K., Lee, Y. B., Cho, H. R., Ghaffari, R., Wang, L., et al. (2016). A graphene-based electrochemical device with thermoresponsive microneedles for diabetes monitoring and therapy. *Nature Nanotechnology, 11*(6), 566.

Li, W., Li, X., Wang, Q., Pan, Y., Wang, T., Wang, H., et al. (2014). Antibacterial activity of nanofibrous mats coated with lysozyme-layered silicate composites via electrospraying. *Carbohydrate Polymers, 99*, 218–225.

Li, W., Luo, X., Song, R., Zhu, Y., Li, B., & Liu, S. (2016). Porous cellulose microgel particle: A fascinating host for the encapsulation, protection, and delivery of Lactobacillus plantarum. *Journal of Agricultural and Food Chemistry, 64*(17), 3430–3436.

Li, W., Zhu, Y., Ye, F., Li, B., Luo, X., & Liu, S. (2017). Probiotics in cellulose houses: Enhanced viability and targeted delivery of Lactobacillus plantarum. *Food Hydrocolloids, 62*, 66–72.

Liu, J., Sun, S., Shang, H., Lai, J., & Zhang, L. (2016). Electrochemical biosensor based on bienzyme and carbon nanotubes incorporated into an Os-complex thin film for continuous glucose detection in human saliva. *Electroanalysis, 28*(9), 2016–2021.

Liu, S., Hui, K., & Hui, K. (2016). Flower-like copper cobaltite nanosheets on graphite paper as high-performance supercapacitor electrodes and enzymeless glucose sensors. *ACS Applied Materials & Interfaces, 8*(5), 3258–3267.

Liu, S., Zhu, Y., Li, W., Li, Y., & Li, B. (2016). Preparation of a magnetic responsive immobilized lipase–Cellulose microgel catalyst system: Role of the surface properties of the magnetic cellulose microgel. *RSC Advances, 6*(9), 7339–7347.

Luo, Z., Lim, S., Tian, Z., Shang, J., Lai, L., MacDonald, B., et al. (2011). Pyridinic N doped graphene: Synthesis, electronic structure, and electrocatalytic property. *Journal of Materials Chemistry, 21*(22), 8038–8044.

Madhu, R., Veeramani, V., Chen, S.-M., Manikandan, A., Lo, A.-Y., & Chueh, Y.-L. (2015). Honeycomb-like porous carbon–cobalt oxide nanocomposite for high-performance enzymeless glucose sensor and supercapacitor applications. *ACS Applied Materials &*

Interfaces, 7(29), 15812–15820.
Moura, M. R., Mattoso, L. H. C., & Zucolotto, V. (2012). Development of cellulose-based bactericidal nanocomposites containing silver nanoparticles and their use as active food packaging. *Journal of Food Engineering, 109*(3), 520–524.
Peng, B., Lu, J., Balijepalli, A. S., Major, T. C., Cohan, B. E., & Meyerhoff, M. E. (2013). Evaluation of enzyme-based tear glucose electrochemical sensors over a wide range of blood glucose concentrations. *Biosensors & Bioelectronics, 49*, 204–209.
Peng, H., Ning, X., Wei, G., Wang, S., Dai, G., & Ju, A. (2018). The preparations of novel cellulose/phenylboronic acid composite intelligent bio-hydrogel and its glucose, pH-responsive behaviors. *Carbohydrate Polymers, 195*, 349–355.
Pereira, L., Amado, A. M., Critchley, A. T., van de Velde, F., & Ribeiro, P. J. A. (2009). Identification of selected seaweed polysaccharides (phycocolloids) by vibrational spectroscopy (FTIR-ATR and FT-Raman). *Food Hydrocolloids, 23*(7), 1903–1909.
Riccardi, C. M., Mistri, D., Hart, O., Anuganti, M., Lin, Y., Kasi, R. M., et al. (2016). Covalent interlocking of glucose oxidase and peroxidase in the voids of paper: enzyme-polymer "spider webs". *Chemical Communication, 52*(12), 2593–2596.
Shan, C., Yang, H., Song, J., Han, D., Ivaska, A., & Niu, L. (2009). Direct electrochemistry of glucose oxidase and biosensing for glucose based on graphene. *Analytical Chemistry, 81*(6), 2378–2382.
Shen, P., & Xia, Y. (2014). Synthesis-modification integration: One-step fabrication of boronic acid functionalized carbon dots for fluorescent blood sugar sensing. *Analytical Chemistry, 86*(11), 5323–5329.
Srinivasan, V., Pamula, V. K., & Fair, R. B. (2004). Droplet-based microfluidic lab-on-a-chip for glucose detection. *Analytica Chimica Acta, 507*(1), 145–150.
Su, L., Feng, J., Zhou, X., Ren, C., Li, H., & Chen, X. (2012). Colorimetric detection of urine glucose based ZnFe2O4 magnetic nanoparticles. *Analytical Chemistry, 84*(13), 5753–5758.
Sun, J., Yao, L., Gao, Z., Peng, S., Wang, C., & Qiu, Y. (2010). Surface modification of PET films by atmospheric pressure plasma-induced acrylic acid inverse emulsion graft polymerization. *Surface & Coatings Technology, 204*(24), 4101–4106.
Vashist, S. K., Lam, E., Hrapovic, S., Male, K. B., & Luong, J. H. (2014). Immobilization of antibodies and enzymes on 3-aminopropyltriethoxysilane-functionalized bioanalytical platforms for biosensors and diagnostics. *Chemical Reviews, 114*(21), 11083–11130.
Wang, H. K., Tsai, C. H., Chen, K. H., Tang, C. T., Leou, J. S., Li, P. C., et al. (2014). Cellulose-based diagnostic devices for diagnosing Serotype-2 dengue fever in human serum. *Advanced Healthcare Materials, 3*(2), 187–196.
Wavhal, D. S., & Fisher, E. R. (2002). Hydrophilic modification of polyethersulfone membranes by low temperature plasma-induced graft polymerization. *Journal of Membrane Science, 209*(1), 255–269.
Wei, H., & Wang, E. (2008). Fe_3O_4 magnetic nanoparticles as peroxidase mimetics and their applications in H_2O_2 and glucose detection. *Analytical Chemistry, 80*(6), 2250–2254.
Wooten, M., Karra, S., Zhang, M., & Gorski, W. (2013). On the direct electron transfer, sensing, and enzyme activity in the glucose oxidase/carbon nanotubes system. *Analytical Chemistry, 86*(1), 752–757.
Wu, K. Y., Chen, C. H., Yeh, C. M., Hwang, J., Liu, P. C., Lee, C. Y., et al. (2005). Liquid-crystal alignment on a-C:H films by nitrogen plasma beam scanning. *Journal of Applied Physics, 98*(8), 083518.
Yan, L., Zhu, Z., Zou, Y., Huang, Y., Liu, D., Jia, S., et al. (2013). Target-responsive "sweet" hydrogel with glucometer readout for portable and quantitative detection of non-glucose targets. *Journal of the American Chemical Society, 135*(10), 3748–3751.
Zhao, Y., Fan, L., Zhang, Y., Zhao, H., Li, X., Li, Y., et al. (2015). Hyper-branched Cu@Cu2O coaxial nanowires mesh electrode for ultra-sensitive glucose detection. *ACS Applied Materials & Interfaces, 7*(30), 16802–16812.